Structural phase transition and phonon instability in Cu_{12}Sb_{4}S_{13}

A. F. May, O. Delaire, J. L. Niedziela, E. Lara-Curzio, M. A. Susner, D. L. Abernathy, M. Kirkham, and M. A. McGuire

Phys. Rev. B **93**, 064104 — Published 8 February 2016

DOI: 10.1103/PhysRevB.93.064104

Structural phase transition and phonon instability in $Cu_{12}Sb_4S_{13}$

A. F. May,[1,*] O. Delaire,[1] J. L. Niedziela,[1] E. Lara-Curzio,[1]
M. A. Susner,[1] D. L. Abernathy,[2] M. Kirkham,[3] and M. A. McGuire[1]

[1]*Materials Science and Technology Division, Oak Ridge National Laboratory, Oak Ridge, TN 37831*
[2]*Quantum Condensed Matter Division, Oak Ridge National Laboratory, Oak Ridge, TN 37831*
[3]*Instrument and Source Division, Oak Ridge National Laboratory, Oak Ridge, TN 37831*

(Dated: January 21, 2016)

A structural phase transition has been discovered in the synthetic tetrahedrite $Cu_{12}Sb_4S_{13}$ at approximately 88 K. Upon cooling, the material transforms from its known cubic symmetry to a tetragonal unit cell that is characterized by an in-plane ordering that leads to a doubling of the unit cell volume. Specific heat capacity measurements demonstrate a hysteresis of more than two degrees in the associated anomaly. Similar hysteresis was observed in powder x-ray diffraction measurements that also indicate a coexistence of the two phases, and together these results suggest a first order transition. This structural transition coincides with a recently-reported metal-insulator transition, and the structural instability is related to the very low thermal conductivity κ in these materials. Inelastic neutron scattering was used to measure the phonon density of states in $Cu_{12}Sb_4S_{13}$ and $Cu_{10}Zn_2Sb_4S_{13}$, both of which possess a localized, low-energy phonon mode associated with strongly anharmonic copper displacements that suppress κ. In $Cu_{12}Sb_4S_{13}$, signatures of the phase transition are observed in the temperature dependence of the localized mode, which disappears at the structural transition. In contrast, in the cubic Zn-doped material the mode is at slightly higher-energy but observable for all temperatures, though it softens upon cooling.

I. INTRODUCTION

Materials that have an intrinsically low lattice thermal conductivity (κ_l) are important for a variety of applications, and finding electrically-tunable materials with low κ_l is key to the search for new thermoelectrics.[1–4] As such, significant effort is placed into understanding the relationships between crystal structure and phonon propagation.[5–7] As one might expect, structurally-unstable materials often have relatively low κ_l. For instance, the ferroelectric instability in PbTe and the orbital (electronic) driven structural transition in SnSe have been linked to their desirable thermoelectric properties.[8–10] These lattice instabilities are associated with strong anharmonicity, which leads to significant phonon-phonon scattering that yields low κ_l. At the same time, structural instabilities need to be understood and controlled, or the desired functionality may not be fully exploited.

Materials related to the mineral known as tetrahedrite ($Cu_{12}Sb_4S_{13}$) possess a very low thermal conductivity ($\kappa \approx 0.5\,W/m/K$ at 300K), which has a temperature dependence more similar to that of amorphous materials than crystalline ones.[11] This low κ allows their thermoelectric figure of merit zT to approach 1 near 700 K.[11–19] Thermoelectric conversion efficiency generally increases with increasing zT of a material, where $zT = \alpha^2\sigma T/\kappa$ contains the Seebeck coefficient α, the electrical conductivity σ, and $\kappa{=}\kappa_l + \kappa_e$ is the thermal conductivity containing both lattice and electronic contributions.

The low thermal conductivity of the tetrahedrites has been linked to large-amplitude displacements of copper atoms,[12] and the presence of nearby Sb atoms appears critical.[20,21] The cubic structure of $Cu_{12}Sb_4S_{13}$ has two copper sites, both with S nearest neighbors; Cu(1) is tetrahedrally coordinated and Cu(2) is in a (slightly-distorted) trigonal planar coordination.[22] The displacements of the Cu(2) atoms are highly anharmonic and anisotropic,[23] and the anisotropic thermal displacement ellipsoids point towards Sb whose lone pair electrons are believed to promote this distortion.[20] Several recent studies have investigated the role of lone-pair s electrons or resonant p-bonds in creating anharmonic environments for atom vibrations.[10,20,24–27] The optical phonons associated with the Cu(2) displacements have been calculated to be unstable, with a double-well atomic potential reported.[12,28] In $Cu_{12}Sb_2Te_2S_{13}$, low-energy phonon modes associated with Cu(2) motion have been observed and are found to display an anomalous softening with decreasing temperature.[21] Low-energy, localized modes like those associated with guest atoms ('fillers/rattlers') in the filled skutterudites or clathrates typically inhibit thermal transport via phonon scattering and/or modifications to phonon dispersions (velocity reduction, phonon localization).[7,29,30]

In addition to interesting lattice dynamics, an electronic phase transition has been reported in $Cu_{12}Sb_4S_{13}$ near 85 K.[11] This is manifested as a metal-insulator transition with a corresponding dip in the magnetic susceptibility upon cooling,[11,31] which is reminiscent of a charge density wave state. The transition is suppressed by a variety of dopants, though its origins have not been identified.[11]

In this work, we reveal that a structural transition occurs at approximately 88 K in synthetic $Cu_{12}Sb_4S_{13}$. The transition is observed in powder x-ray diffraction data as

a splitting of Bragg peaks and the emergence of additional reflections, which indicate a tetragonal structure at low temperatures. Powder x-ray diffraction and specific heat measurements suggest that the transition is first order. To examine the lattice dynamics in further detail, the phonon density of states was probed with inelastic neutron scattering (INS), which has proven particularly powerful for yielding detailed insights into phonon dynamics and scattering.[8–10,32–37] The INS measurements show the existence of a low-energy vibration mode in the high-temperature cubic phase, which disappears at the structural transition in $Cu_{12}Sb_4S_{13}$. With Zn doping, the high-temperature cubic structure is stabilized and this mode shifts to a higher energy, but displays anomalous softening on cooling.

II. EXPERIMENTAL DETAILS

Synthetic $Cu_{12}Sb_4S_{13}$ and $Cu_{12-x}Zn_xSb_4S_{13}$ ($x = 1, 2$) were prepared by direct reaction of high-purity elements in sealed quartz ampoules. The elements were slowly heated in a quartz ampoule to 650 °C and held for 12-36 h. The resulting material was ball milled for 40 min under He, then annealed at 450 °C for a minimum of 4 d (x=0,2 for inelastic neutron scattering) and a maximum of 17 d ($x = 1$ for powder x-ray diffraction). The loading and unloading of the milling vial were performed in a He glove box.

Powder x-ray diffraction measurements were performed from 300 K to 20 K, using a PANalytical X'Pert Pro MPD with a Cu $K_{\alpha,1}$ incident-beam monochromator. Rietveld and Le Bail refinements were performed using FullProf.[38]

The primary impurity phases in our $Cu_{12}Sb_4S_{13}$ samples are Cu_3SbS_4 and an enlarged tetrahedrite phase (both $\lesssim 3\%$). The enlarged tetrahedrite phase is extremely difficult to avoid in the ternary system. It is formed during an exsolution reaction below $\approx$95 °C, where a homogeneous tetrahedrite matrix separates into copper rich (near $Cu_{14}Sb_4S_{13}$) and copper 'poor' regions (near $Cu_{12}Sb_4S_{13}$) that both possess the cubic tetrahedrite structure.[39,40] It was reported by Tatsuka and Morimoto that the diffusion coefficient of copper in tetrahedrite is large enough at room temperature to allow the reversible formation of these two phases in the presence of excess copper or sulfur.[39] From Le Bail fits, the lattice parameter of the enlarged unit cell phase in our undoped material is found to be 10.4431(10) Å and 10.4149(9) Å at 300 and 20 K, respectively. We emphasize that the phase transition is observed in the small-cell tetrahedrite, which dominates the volume fraction of our samples. The addition of Zn leads to purer samples, and in the cases of $Cu_{11}ZnSb_4S_{13}$ and $Cu_{10}Zn_2Sb_4S_{13}$ our laboratory powder x-ray diffraction does not detect the enlarged tetrahedrite cell. This appears to be similar to the influence other divalent (or trivalent) dopants,[18,41] which suppress the exsolution into two tetrahedrite phases.

Specific heat capacity measurements were performed using a Quantum Design Physical Property Measurement System. These measurements revealed the first order nature of the phase transition. To probe this behavior, large heat pulse measurements were performed and Quantum Design's single slope analysis tool was employed.

Inelastic neutron scattering (INS) spectra were measured using the ARCS time-of-flight chopper spectrometer at the Spallation Neutron Source, at Oak Ridge National Laboratory.[42] The samples were encased in thin-walled cylindrical Al containers, 12 mm in diameter. For measurements at low temperatures, the sample holder was cooled by a closed-cycle He refrigerator. We used two incident neutron energies $E_\mathrm{i} = 20$ and 70 meV. The energy resolution (full width at half maximum) for $E_\mathrm{i} = 20$ meV was about 0.55 meV at 10 meV neutron energy loss, increasing to about 1.0 meV at the elastic line. The empty Al sample container was measured in identical conditions at all temperatures.

All spectra were normalized by the total incident flux, and corrected for detector efficiency. In all cases, the spectrum from the empty sample container was subtracted. The analysis of the phonon DOS was performed in the incoherent scattering approximation, using the MANTID software.[43] This approximation works well in the case of powder samples, when the scattering conditions allow the sampling of multiple Brillouin zones in reciprocal space, which was the case in our measurements. The elastic peak was removed, and the data below 1.9 meV (3 meV) for $E_\mathrm{i} = 20$ meV ($E_\mathrm{i} = 70$ meV) were extrapolated using a Debye model. A standard procedure was used to correct for the effect of multiphonon scattering.[44]

For single-phonon scattering in a polyatomic material, the inelastic neutron scattering cross-section is proportional to the scattering function,

$$S(Q,E) = \sum_i \sigma_i \frac{\hbar^2 Q^2}{2m_i} \exp(-2W_i) \frac{g_i(E)}{E} [n_T(E)+1] \,,$$

where Q and E are the momentum and energy transfer to the sample, σ_i, m_i, and $\exp(-2W_i)$ are the neutron scattering cross-section, mass, and Debye-Waller factor for atom i, respectively, and $n_T(E)$ is the Bose occupation factor.[45] The partial phonon DOS, g_i, is defined as

$$g_i(E) = \sum_{j,\boldsymbol{q}} |e_i(j,\boldsymbol{q}))|^2 \delta[E - E(j,\boldsymbol{q})] \,,$$

where $E(j,\boldsymbol{q})$ and $e(j,\boldsymbol{q})$ are the phonon energies and eigenvectors.[45,46] Because different isotopes have different factors σ/M, the modes corresponding to the elements of higher scattering efficiency are over-emphasized over those of elements with lesser neutron scattering efficiency, resulting in a skewed generalized phonon DOS. The values of σ/M for Cu, Zn, Sb, and S are 0.126, 0.063, 0.032, and 0.032, respectively. Thus, the modes involving large motions of Cu atoms are overemphasized in the measured phonon spectra. This effect should be taken

into account when comparing with lattice dynamics simulations.

III. RESULTS AND DISCUSSION

A. Structural Phase Transition

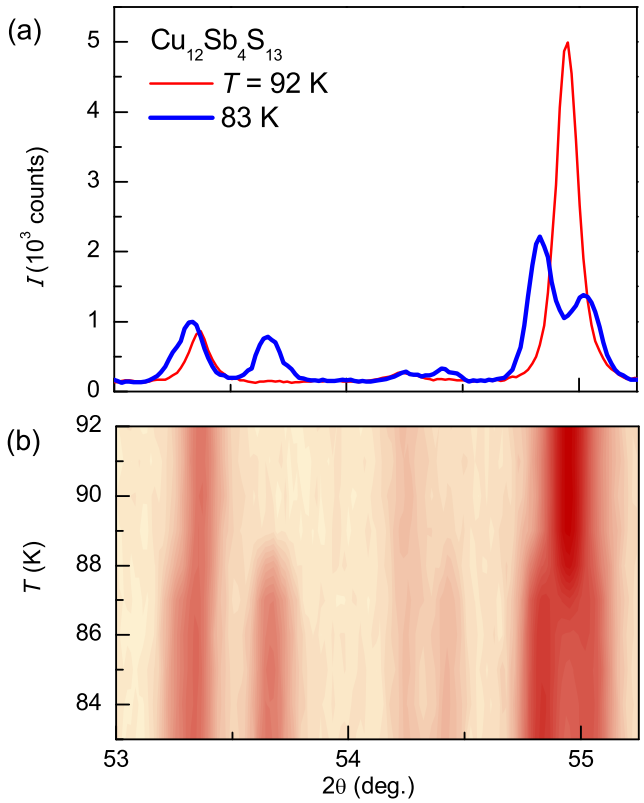

FIG. 1: Temperature dependent powder x-ray diffraction data collected on cooling (λ=1.5406 Å) across the structural phase transition in $Cu_{12}Sb_4S_{13}$. The splitting of Bragg peaks reveals the transition from cubic to tetragonal symmetry upon cooling, and the emergence of additional reflections relates to the enlargement of the cell.

The phase transition is observed in Fig. 1 by the splitting of cubic Bragg peaks and the emergence of additional peaks. This is seen to occur near 88 K based on our powder x-ray diffraction data, which is consistent with literature reports of a metal-insulator transition and our specific heat capacity measurements (below). All additional reflections are indexed by a $\sqrt{2} \times \sqrt{2}$ expansion of the *ab*-plane, and this supercell formation results in a tetragonal lattice at low temperature. On warming, the ordered state is disrupted by thermal displacements and the structure relaxes into a cubic state with high entropy.

The structural distortion is suppressed by doping, as shown by the temperature-dependent lattice parameters for undoped $Cu_{12}Sb_4S_{13}$ and two Zn doped samples in Fig. 2. To facilitate the viewing of these results, the basal plane lattice parameter of the tetragonal cell (a_{tet}) has been divided by $\sqrt{2}$. This plot also demonstrates the expansion of the lattice with Zn doping, which is consistent with prior reports.[47] The lattice parameters obtained by Le Bail refinements are summarized in Table I.

Figure 2 also reveals that Zn-doping reduces the thermal expansion coefficient of $Cu_{12-x}Zn_xSb_4S_{13}$. The coefficients of linear thermal expansion (α_T) obtained from our diffraction data are shown in Table I. Here, we defined $\alpha_T = \frac{a(300K)-a(200K)}{a(300K)\Delta T}$. The suppression of α_T highlights the stabilization of the lattice with Zn-doping. Even with Zn doping, the lattice anharmonicity remains, and a region of negative thermal expansion is observed at low temperatures for the $Cu_{10}Zn_2Sb_4S_{13}$ sample. The lattice parameter of $Cu_{10}Zn_2Sb_4S_{13}$ begins to plateau below approximately 100 K, and upon cooling from 60 to 20 K a increases from 10.3669(3) to 10.3675(3) Å. We note that the reported α_T value for x=0 is similar to those of the high temperature thermoelectric materials $La_{3-x}Te_4$ and $Yb_{14}MnSb_{11}$.[35,48,49]

Figure 3 shows x-ray powder diffraction data collected at 20 K on $Cu_{12}Sb_4S_{13}$ in the tetragonal phase. A Rietveld refinement is shown, and the associated lattice parameters are provided in the Figure. During the fit, the excluded regions were utilized to eliminate diffraction peaks from the sample holder.

A structural model for the low temperature phase can be constructed by starting with a tetragonal $\sqrt{2} \times \sqrt{2} \times 1$ supercell of the high temperature, cubic structure. In this tetragonal cell, the cubic structure can be reproduced exactly using space group $P\overline{4}$. Higher symmetry tetragonal space groups were tested, but none were consistent with the room temperature structural framework. This model contains 14 Cu sites, 4 Sb sites, and 15 S sites. Note that at this level of approximation, the model still has cubic symmetry, although the imposed supercell is tetragonal. It is the movement of atoms away from sites that are symmetry constrained in the high temperature structure that lowers the crystal symmetry from cubic to tetragonal, thus requiring the $\sqrt{2} \times \sqrt{2}$ description of the *ab*-plane while also producing the observed superlattice reflections (Fig. 1). When this occurs, c is no longer constrained to equal $\sqrt{2}a$, which results in the splitting of the subcell Bragg peaks.

In the low temperature model, there are 83 atomic position parameters that are unconstrained by symmetry. This presents a significant challenge for crystallographic analysis using powder diffraction. Single crystal diffraction data were collected at 50 K and showed the crystallographic distortion, but strong twinning that occurs upon cooling into the tetragonal phase precluded further analysis. To aid in the refinement of the powder diffraction data, soft constraints were imposed to maintain reasonable interatomic distances. Due to the structural complexity, a complete description of the structure is difficult to obtain from the present data. Importantly, however, Fig. 3 shows that the intensities of superlattice reflections

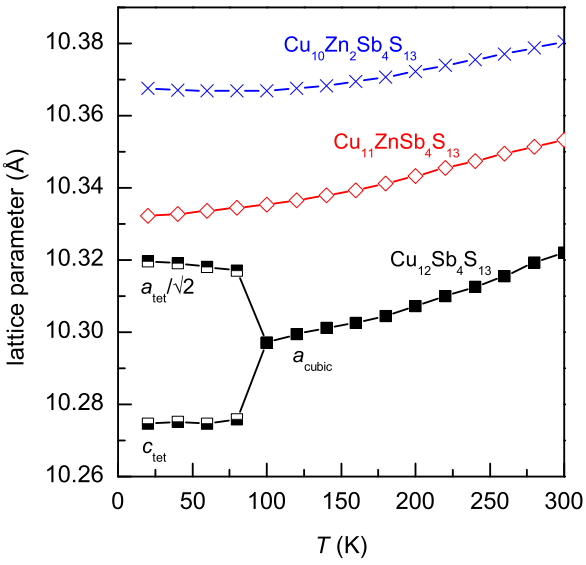

FIG. 2: Temperature dependent lattice parameters obtained from powder x-ray diffraction data revealing the phase transition in $Cu_{12}Sb_4S_{13}$, along with data for cubic phases $Cu_{11}ZnSb_4S_{13}$ and $Cu_{10}Zn_2Sb_4S_{13}$.

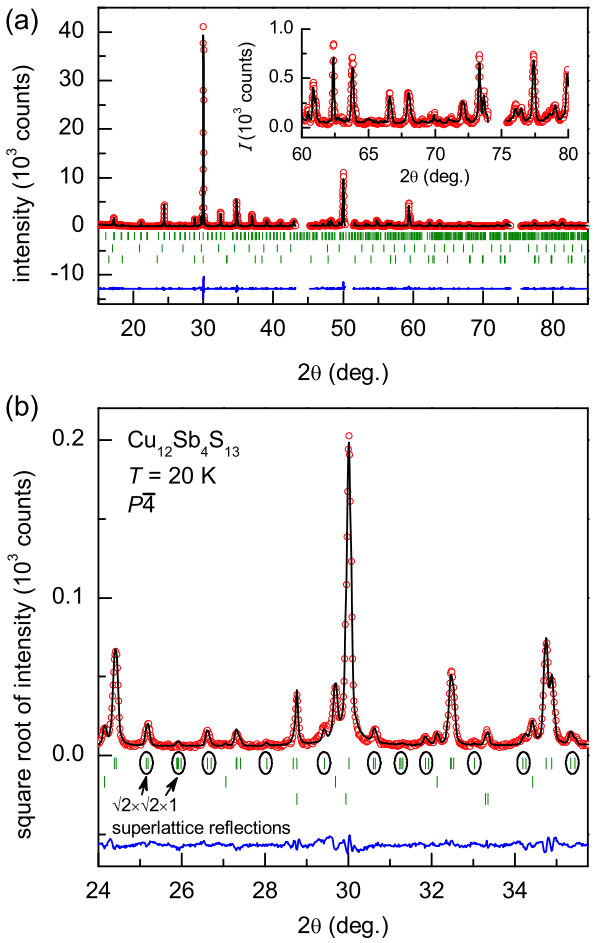

FIG. 3: Rietveld refinement of x-ray diffraction data collected at 20 K for $Cu_{12}Sb_4S_{13}$. The green tick marks indicate locations of Bragg reflections for the small unit cell tetrahedrite phase in the tetragonal structure (upper), the large unit cell tetrahedrite phase in the cubic structure (middle), and Cu_3SbS_4 (lower).

are matched reasonably well, indicating that the model used is sufficient to describe the data. The lattice parameters determined from the refinement of data collected at 300 K and 20 K are listed in Table I.

A detailed discussion of the refined structure is unwarranted because of the limitations noted above, but qualitative observations can be made. As previously discussed, it is expected that structural instabilities in $Cu_{12}Sb_4S_{13}$ are related to displacements of trigonally coordinated Cu atoms.[12] In the model used here, 8 of the 14 Cu sites are in trigonal coordination by S. Four of these are on special positions that constrain them to be coplanar with their surrounding S triangle. Of the four Cu atoms where such a symmetry constraint does not exist, three are displaced away from their planar positions. One Cu site shows a significant distortion, moving more than 0.3 Å out of the plane defined by the three coordinating S atoms and to within 3.0 Å of a neighboring Sb. For comparison, the other Cu−Sb distances in the structure are greater than 3.3 Å and the closest Cu−Sb contact in the room temperature structure is about 3.4 Å. Thus, although the full details of the low temperature structure are not known, it is apparent that displacements of trigonally coordinated Cu are involved in the structural transition.

B. Evidence for a First Order Transition

The order of the transition is now considered through specific heat measurements and diffraction data collected on warming and cooling through the transition, both of which are shown in Fig. 4. The specific heat capacity measurement shows a hysteresis of ≈ 2.6 K, as observed in Fig. 4(a). The raw data for this measurement are shown in the inset of Fig. 4(a), which shows the time dependence of the sample T with constant heater power for 108 s. A latent heat associated with the phase transition can be observed as the plateaus on warming and cooling. The heating portion of the curve has this anomaly at higher temperature than does the cooling curve, and this pulse measurement provides a quick demonstration of the hysteresis and latent heat.

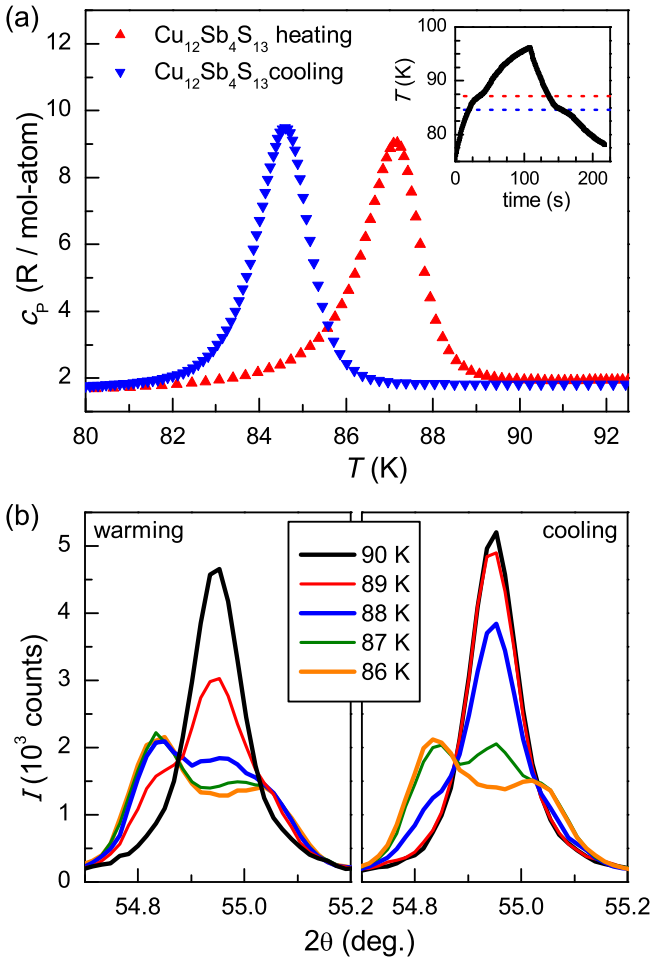

FIG. 4: (a) Specific heat capacity data contain a hysteresis between heating and cooling curves, and the raw data (inset) demonstrate that the transition has an associated latent heat. (b) Powder diffraction through the transition also reveals hysteresis between heating and cooling curves, as well as an indication of coexistence between the high- and low-temperature phases.

Figure 4(b) shows diffraction data collected on warming and cooling through the transition. These data also show a hysteresis of approximately 2 K, consistent with the specific heat measurements. When examined closely, the diffraction data also suggest a coexistence of both phases. Three peaks can be observed at 87 K on cooling (or 88 K on warming), where the outer two (tetragonal) peaks come from the splitting of the central (cubic) peak. The locations of the Bragg peaks are consistent and fairly well defined, and the hysteresis is in general agreement (within resolution) of that observed in the specific heat measurement. Therefore, we do not believe these results are due to inhomogeneity of the sample (chemical or thermal). As such, these results provide evidence that the transition is of first order.

Care must be taken when collecting and analyzing specific heat capacity data across a first order phase transition. When performing measurements in a Quantum Design PPMS using the standard specific heat option, the presence of latent heat leads to significant errors in the analyzed results. These data were obtained using a heat pulse producing a temperature rise of 30% of the temperature setpoint and a long collection time (∼4 time constants). The data were subsequently analyzed using Quantum Design's single slope method analysis tool, which analyzes heating and cooling curves separately and is designed for treating first order transitions. As such, the features on warming and cooling are well resolved. We note that the entropy change across the transition, obtained by integrating c_P/T, is found to be ΔS=4.7 R and 4.5 R on heating and cooling, respectively. For this integration, a baseline was manually selected and c_P/T does not contain a strong temperature dependence in this region except for the anomaly itself.

TABLE I: Lattice parameters for the $Cu_{12-x}Zn_xSb_4S_{13}$ samples at 300 and 20 K. The linear coefficients of thermal expansion (α_T) are obtained using lattice parameters at 200 and 300 K, since they vary nearly linearly with temperature in all samples near room temperature (Fig. 2).

sample	a_{300K} Å	a_{20K} Å	c_{20K} Å	α_T 10^{-5}K^{-1}
$Cu_{12}Sb_4S_{13}$	10.3221(3)	14.5941(5)	10.2746(4)	1.43
$Cu_{11}ZnSb_4S_{13}$	10.3533(2)	10.3323(3)	$=a$	0.98
$Cu_{10}Zn_2Sb_4S_{13}$	10.3805(4)	10.3675(3)	$=a$	0.80

C. Lattice Dynamics

The generalized phonon DOS obtained from the ARCS measurements at 200 K are shown in Fig. 5 for $Cu_{12}Sb_4S_{13}$ and $Cu_{10}Zn_2Sb_4S_{13}$. Overall, the phonon DOS is similar for the two compositions. The maximum phonon energy is about 48 meV, located at the top of a wide band of optical modes likely involving predominantly the light sulfur atoms at $30 \leqslant E \leqslant 48$ meV, as predicted in Ref. 12,20. We note that sulfur vibrations are under-weighted in our generalized DOS measurements, leading to lower intensity in this energy range than in simulations.[12,20] In addition, several peaks are observed at $E \sim 19$ meV, 9 meV, and below 4 meV. While the lowest energy peak only appears as a shoulder in our measurements with $E_i = 70$ meV, it is clearly resolved in the higher-resolution measurements with $E_i = 20$ meV. By comparing with reported simulations[12,20], we can identify the peak below 4 meV with a low-energy optical vibration mode of trigonally-bonded Cu atoms. This feature is in very good agreement with measurements reported by Bouyrie *et al.* in $Cu_{12}Sb_2Te_2S_{13}$.[21] The agreement on the existence of this low energy mode confirms the importance of Sb bonding in the tetrahedrite structure, since this peak is absent in measurements of $Cu_{10}Te_4S_{13}$ (Ref. 21). The role of the Sb lone-pairs in producing an unstable bonding environment was also highlighted in

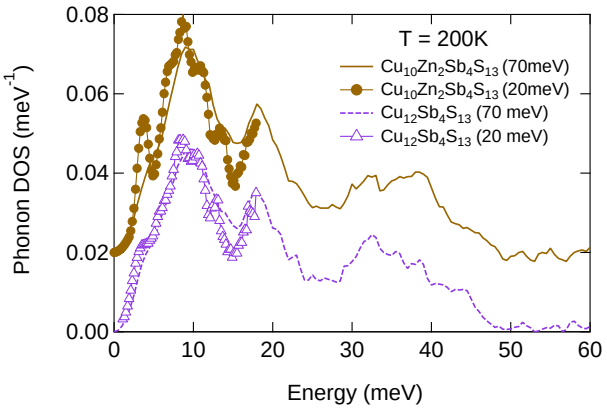

FIG. 5: Phonon DOS of $Cu_{12}Sb_4S_{13}$ and $Cu_{10}Zn_2Sb_4S_{13}$ at 200 K, measured by inelastic neutron scattering. The lines are for the measurements performed with $E_i = 70$ meV, which are corrected for multiphonon scattering. Markers are for the high-resolution measurements with $E_i = 20$ meV, which only sampled the low-energy portion of the DOS, and were not corrected for multiphonon scattering (see text).

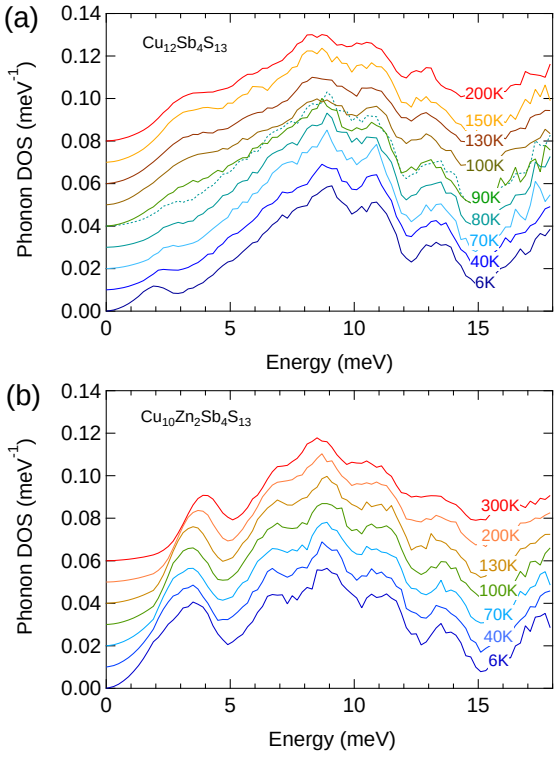

FIG. 6: Temperature dependence of the phonon DOS from INS measurements for (a) $Cu_{12}Sb_4S_{13}$ and (b) $Cu_{10}Zn_2Sb_4S_{13}$. Curves for different temperatures are vertically offset for clarity. In panel (a) the curve for $T = 80$ K is replicated (dots) with the same offset as for the curve for $T = 90$ K, in order to highlight the discontinuous change in shape at the structural phase transition.

Refs. 12,20.

While the phonon DOS are generally similar for the doped and undoped material, there are significant differences in the low-energy mode(s) observed near 2-4 meV. In particular, the temperature dependence of this mode is clearly different, as shown in Fig. 6 where data obtained using $E_i = 20$ meV are plotted. In the undoped material, the low-energy mode disappears at the structural transition and then re-appears at lower energy in the tetragonal phase (Fig. 6(a)). In the Zn-doped material, which remains cubic, decreasing temperature leads to a striking softening and broadening of the low-energy peak.

We fitted the energies of peaks from the $E_i = 20$ meV data at $\sim$ 3 meV (peak 1), $\sim$ 8 meV (peak 2), and $\sim$ 18 meV (peak 3) as a function of temperature and the results are shown in Fig. 7. For peak 1, we used a combination of a Gaussian and parabola, over the range $0 \leqslant E \leqslant 6$ meV, while peaks 2 and 3 were fitted with a single Gaussian and a flat background over a window of 2.5 meV and 5 meV, respectively, around the peak center. The mode widths reported in Fig. 7 are full-width-at-half-maximum and are corrected for the estimated experimental instrument resolution.

A softening of phonons with decreasing temperature is opposite to the quasi-harmonic (QH) behavior that is typically observed in most materials. In the QH model, phonon frequencies depend on temperature solely through the change in volume of the system and one can define a T-independent Grüneisen parameter $\gamma = -d\ln E/d\ln V$ to describe this behavior. Typically, γ is positive and one expects a decrease (softening) in phonon frequencies with increasing temperature due to thermal expansion, $\Delta E/E = -\gamma\,\Delta V/V$ (or equivalently, an increase in phonon frequency upon cooling). The temperature dependence of the peaks at $E \sim 9$ meV and 18 meV follows the expected trend from thermal expansion in the QH approximation. However, this is opposite to the behavior observed for the low-energy optic mode in the tetrahedrites, which shows a pronounced softening on cooling, revealing strong anharmonicity near a structural instability. This temperature dependence is especially clear in the Zn-doped sample. Looking at the temperature evolution of the DOS in Fig. 6, one can also notice that features in the range $6 \leqslant E \leqslant 15$ meV exhibit some broadening upon heating, which is typical of anharmonic scattering as vibrational amplitudes increase.

As can be seen in Fig. 7, the low-energy optic mode for trigonal Cu atoms in $Cu_{10}Zn_2Sb_4S_{13}$ softens from 3.8 meV at 300 K to 2.6 meV at 6 K. Also, the width of the mode increases significantly upon cooling. This behavior is consistent with that observed in $Cu_{12}Sb_2Te_2S_{13}$.[21] The behavior of the low-energy optical mode in $Cu_{12}Sb_4S_{13}$ is quite different. At 200 K, the mode frequency is $\approx$ 3.1 meV, lower than that in $Cu_{10}Zn_2Sb_4S_{13}$ ($\approx$ 3.5 meV) for the same temperature. Overall, this mode(s) associated with the trigonal Cu(2) is broader in the undoped sample, indicative of stronger damping. Between 100 K and 200 K, the mode frequency remains

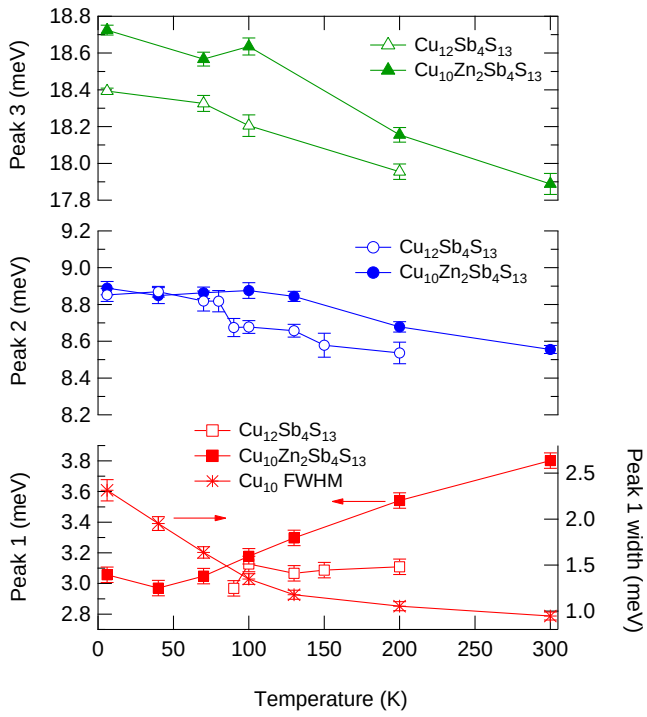

FIG. 7: Temperature dependence of phonon energies for peak 1 ($E \simeq 3$ meV), peak 2 ($E \simeq 9$ meV), and peak 3 ($E \simeq 18$ meV). The width of peak 1 is FWHM, corrected for instrument resolution.

constant $E \simeq 3.06 \pm 0.10$ meV, consistently lower than in $Cu_{10}Zn_2Sb_4S_{13}$. The mode responds strongly to the structural transition in the undoped sample, with peak 1 abruptly disappearing between 90 K and 80 K. Below the transition temperature, a weaker mode appears at ~ 2 meV and softens on further cooling to 6 K. We also note that peaks 2 and 3 at higher energy follow the regular softening on heating expected within the QH approximation. Still, for both compounds, the temperature dependence of these peaks is quite strong. Using the experimentally determined lattice parameters, we estimate a Grüneisen parameter close to 10. The apparent discontinuity in the energy of peak 2 in the undoped sample between 80 and 90 K could be associated with the structural distortion. In addition, above the transition, the energies of peaks 2 and 3 are stiffer (by about 2 %) in the Zn-doped sample compared to the undoped tetrahedrite. This stiffening upon alloying likely reflects the stiffening of force-constants upon filling of holes with doping, which suppresses electronic screening of atomic displacements.[35] We note that this stiffening is much stronger for peak 1 (about 15 % at 200 K), indicating that the trigonal Cu environment may be most sensitive to the changes in bonding upon Zn doping.

Overall, the behavior of the low-energy optical mode associated with trigonally-bonded Cu atoms is reminiscent of a soft-mode instability, as seen for example in the rock-salt chalcogenides and in SnSe[8–10,50,51]. However, in the tetrahedrites, the anharmonic low-energy optical mode is Einstein-like: it must have little dispersion, with E almost independent of $\boldsymbol{q}$ in order to build up sufficient spectral weight to give rise to a pronounced peak in the phonon DOS (following convention, we refer to the entire flat branch as a single Einstein mode, although it is really a collection of modes at the same energy). This is compatible with the observation of a near dispersionless branch at ~ 4 meV in the single-crystal data on a natural tetrahedrite sample reported by Bouyrie *et al.*, Ref. 21. This is in contrast to the strongly dispersive zone-center soft-modes observed in rocksalt chalcogenides and SnSe. This dispersionless behavior is indicative of a localized instability of the trigonal Cu vibrations, which are decoupled and vibrate incoherently from one another instead of forming a collective dispersive band. As a result, we do not expect to observe a well-defined phonon wave vector at which the mode would fully soften. The Einstein-like character of the trigonal Cu vibrations also leads to a definite enhancement in the low-temperature heat capacity, as previously reported.[52] This view is also supported by the first-order character of the structural phase transition observed in our specific heat and diffraction measurements. The strongly anharmonic character of the trigonal Cu vibrations is manifest in the pronounced softening on cooling reported here, and was also inferred from an anharmonic refinement of the atomic displacement parameters from single-crystal x-ray diffraction.[23] The strong anharmonicity of this low-energy optical mode was shown to arise from the unstable bonding environment provided by the Sb lone pairs,[20] and likely contributes to achieving the very low $\kappa_{\rm lat}$.[21]

The changes in the phonon DOS between the undoped and doped tetrahedrite shed light on the stability of the lattice. That is, the stiffer frequency for this mode(s) in the Zn-doped sample demonstrates the stabilization of the lattice by Zn-substitution (a transition could be expected at $T < 0$ K when the mode fully softens, in analogy to incipient ferroelectrics like PbTe). Substitutional impurities are known to strongly suppress the phase transition of $Cu_{12-x}M_xSb_4S_{13}$ compounds, where M is a divalent or trivalent transition metal.[11] In the case of Fe and Ni-doping, these substitutions have been found to stabilize the structure at higher temperatures, potentially widening the range over which these materials can be utilized for thermoelectric power generation.[18,41] It is believed that the transition metal impurities reside primarily on the tetrahedrally coordinated Cu(1) position.[17,18,53] Thus, the suppression of the transition does not appear to be directly related to the disorder induced by the substitutions since the Cu(2) position appears to dominate the transition. Also, the change in unit cell volume does not appear critical. While the lattice expands with Zn or Fe doping, very little change in the lattice parameter is observed upon Ni-doping and low temperature transport measurements suggest that Ni-doping suppresses the transition.[11,47] In addition, considering only the effects of the quasi-harmonic model dis-

cussed above one would expect the lattice expansion to soften the phonons (this is a simplification due to changing atomic species). However, Zn-doping leads to a stiffening of the phonons. This stiffening may be due to a reduction in the screening of ionic displacements that can occur when the free carrier concentration decreases (as Zn content increases).[35] Therefore, since this structural transition appears to be strongly coupled to a previously reported electronic phase transition,[11] the filling of empty valence band states upon doping likely stabilizes the cubic phase. Detailed simulations of the influence of doping on the bonding in these materials are required to make a definitive statement about the stabilizing effect of dopants.

The stiffening of the low-energy mode and the change in its temperature dependence upon doping may have less obvious influences on the lattice dynamics and associated transport properties. The frequency of an isolated mode strongly influences the way in which it interacts with the dispersive, acoustic phonons of the lattice that carry the majority of the heat. The isolated mode can either scatter these phonons or modify their dispersions.[7] As such, understanding the way in which modes interact and change with doping and temperature allows for a more complete picture of phonon transport and can aid in the design and development of new materials for thermal management or thermoelectric applications.

IV. SUMMARY

In summary, we have shown that the heavily-characterized thermoelectric material $Cu_{12}Sb_4S_{13}$ undergoes a first-order crystallographic phase transition near 88 K, and that it is likely driven by Cu displacements towards neighboring Sb. In the high temperature (cubic) phase, copper displacements are known to be highly anharmonic and lead to the low thermal conductivity that is favorable for thermoelectric energy conversion. In the low temperature (tetragonal) phase, however, the lattice is stabilized through an apparent increase in Cu-Sb bonding and a corresponding supercell formation. This structural phase transition is coupled with the previously reported metal-insulator transition. Our inelastic neutron scattering results demonstrate the existence of a low-energy phonon mode that reacts strongly to the phase transition. The stabilization of the lattice via Zn-doping is observed as a stiffening of this localized mode. The ability to tune the location of this low-energy mode via doping, either isoelectronic or aliovalent, may provide a means to enhance the strong phonon-phonon scattering that leads to such low thermal conductivity in these materials. As such, this study reveals a coupling between the lattice instability and electronic structure that allows for favorable thermoelectric properties.

V. ACKNOWLEDGEMENTS

This work (A.F.M., M.A.S, M.A.M.) was supported by the U. S. Department of Energy, Office of Science, Basic Energy Sciences, Materials Sciences and Engineering Division. Neutron scattering measurements and analysis (O.D., J.N.) were supported as part of the S3TEC EFRC, an Energy Frontier Research Center funded by the U.S. Department of Energy, Office of Science, Basic Energy Sciences under Award # DE-SC0001299. This study was supported in part (E.L.C.) through the Center on Revolutionary Materials for Solid State Energy Conversion, an Energy Frontier Research Center funded by the U. S. Department of Energy, Office of Basic Energy Sciences under Award No. DE-SC0001054. The Research at Oak Ridge National Laboratory's Spallation Neutron Source was sponsored by the Scientific User Facilities Division, Office of Basic Energy Sciences, US DOE.

* Electronic address: mayaf@ornl.gov

[1] G. D. Mahan, *Solid State Physics*, vol. 51 (Academic Press, New York, 1998).
[2] C. Wood, Rep. Prog. Phys. **51**, 459 (1988).
[3] J. R. Sootsman, D. Y. Chung, and M. G. Kanatzidis, Angew. Chem. Int. Ed. **48**, 8616 (2009).
[4] E. S. Toberer, A. F. May, and G. J. Snyder, Chem. Mater. **22**, 624 (2010).
[5] G. A. Slack, *Solid State Physics*, vol. 34 (Academic Press, New York, 1979).
[6] E. S. Toberer and G. J. Snyder, Nat. Mater. **7**, 105 (2008).
[7] E. S. Toberer, A. Zevalkink, and G. J. Snyder, J. Mater. Chem. **21**, 15843 (2011).
[8] O. Delaire, J. Ma, K. Marty, A. F. May, M. A. McGuire, M.-H. Du, D. J. Singh, A. Podlesnyak, G. Ehlers, M. D. Lumsden, et al., Nat. Mater. **10**, 614 (2011), URL http://www.nature.com/nmat/journal/v10/n8/full/nmat3035.html.
[9] C. W. Li, O. Hellman, J. Ma, A. F. May, H. B. Cao, X. Chen, A. D. Christianson, G. Ehlers, D. J. Singh, B. C. Sales, et al., Phys. Rev. Lett. **112**, 175501 (2014), URL http://link.aps.org/doi/10.1103/PhysRevLett.112.175501.
[10] C. Li*, J. Hong*, A. F. May, D. Bansal, J. Ma, T. Hong, S. Chi, G. Ehlers, and O. Delaire, Nat. Phys. **11**, 1063 (2015).
[11] K. Suekuni, K. Tsuruta, and M. Ariga, T amd Koyano, App. Phys. Exp. **5**, 051201 (2012), ISSN 0021-8979.
[12] X. Lu, D. T. Morelli, Y. Xia, F. Zhou, V. Ozolins, H. Chi, X. Zhou, and C. Uher, Adv. Funct. Mater. **3**, 342 (2013).
[13] K. Suekuni, K. Tsuruta, M. Kunii, H. Nishiate, E. Nishibori, S. Maki, M. Ohta, A. Yamamoto, and M. Koyano, J. Appl. Phys. **113**, 043712 (2013).
[14] X. Lu and D. Morelli, Phys. Chem. Chem. Phys. **15**, 5762 (2013).
[15] X. Lu and D. Morelli, MRS Commun. **3**, 129 (2013).
[16] X. Lu and D. Morelli, J. Electron. Mater. **43**, 1983 (2014).
[17] R. Chetty, D. Kumar, G. Rogl, P. Rogl, E. Bauer, H. Mi-

chor, S. Suwas, S. Puchegger, G. Giester, and R. Mallik, Phys. Chem. Chem. Phys. **17**, 1716 (2015).
[18] T. Barbier, P. Lemoine, S. Gascoin, O. Lebedev, A. Kaltzoglou, P. Vaqueiro, A. Powell, R. Smith, and E. Guilmeau, J. Alloy. Compd. **634**, 253 (2015).
[19] X. Lu, D. Morelli, Y. Xia, and V. Ozolins, Chem. Mater. **27**, 408 (2015).
[20] W. Lai, Y. Wang, D. Morelli, and X. Lu, Adv. Funct. Mater. **25**, 3648 (2015).
[21] Y. Bouyrie, C. Candolfi, S. Pailhés, M. M. Koza, B. Malaman, A. Dauscher, J. Tobola, O. Boisron, L. Saviot, and B. Lenoir, Phys. Chem. Chem. Phys. **17**, 19751 (2015).
[22] B. J. Wuensch, Z. Kristallogr. **119**, 437 (1964).
[23] A. Pfitzner, M. Evain, and V. Petricek, Acta Cryst. **B53**, 337 (1997).
[24] E. J. Skoug and D. T. Morelli, Phys. Rev. Lett. **107**, 235901 (2011).
[25] Y. Zhang, E. Skoug, J. Cain, V. Ozoliņš, D. Morelli, and C. Wolverton, Phys. Rev. B **85**, 054306 (2012), URL `http://link.aps.org/doi/10.1103/PhysRevB.85.054306`.
[26] M. Nielsen, V. Ozolins, and J. Heremans, Energ. Environ. Sci. **6**, 570 (2013).
[27] S. Lee, K. Esfarjani, T. Luo, J. Zhou, Z. Tian, and G. Chen, Nat. Commun. **5**, 3525 (2014).
[28] F. Zhou, W. Nielson, Y. Xia, and V. Ozoliņš, Phys. Rev. Lett. **113**, 185501 (2014), URL `http://link.aps.org/doi/10.1103/PhysRevLett.113.185501`.
[29] T. Takabatake, K. Suekuni, T. Nakayama, and E. Nakayama, Rev. Mod. Phys. **86**, 669 (2014).
[30] S. Pailhès, H. Euchner, V. M. Giordano, R. Debord, A. Assy, S. Gomès, A. Bosak, D. Machon, S. Paschen, and M. de Boissieu, Phys. Rev. Lett. **113**, 025506 (2014), URL `http://link.aps.org/doi/10.1103/PhysRevLett.113.025506`.
[31] F. DiBenedetto, G. P. Bernardini, C. Cipriani, C. Emiliani, D. Gatteschi, and M. Romanelli, Phys. Chem. Minerals **32**, 155 (2005).
[32] V. Keppens, D. Mandrus, B. Sales, B. Chakoumakos, P. Dai, R. Coldea, M. Maple, D. Gajewski, E. Freeman, and S. Bennington, Nature **395**, 876 (1998).
[33] M. Koza, M. Johnson, R. Viennois, H. Mutka, L. Girard, and D. Ravot, Nat. Mater. **7**, 805 (2008).
[34] M. Christensen, A. Abrahamsen, N. Christensen, F. Juranyi, N. Andersen, K. Lefmann, J. Andreasson, C. Bahl, and B. Iversen, Nat. Mater. **7**, 811 (2008).
[35] O. Delaire, A. F. May, M. A. McGuire, W. D. Porter, M. S. Lucas, M. B. Stone, D. L. Abernathy, V. Ravi, S. A. Firdosy, and G. J. Snyder, Phys. Rev. B **80**, 184302 (2009).
[36] J. Ma, O. Delaire, A. May, C. Carlton, M. McGuire, L. VanBebber, D. Abernathy, G. Ehlers, T. Hong, A. Huq, et al., Nat. Nanotech. **8**, 445 (2013).
[37] D. Voneshen, K. Refson, E. Borissenko, M. Krisch, A. Bosak, A. Piovano, E. Cemal, M. Enderle, M. Gutmann, M. Hoesch, et al., Nat. Mater. **12**, 1028 (2013).
[38] J. Rodrguez-Carvajal, Physica B **192**, 55 (1993).
[39] K. Tatsuka and N. Morimoto, Am. Mineral. **58**, 425 (1973).
[40] E. Makovicky and B. Skinner, Can. Mineral. **16**, 611 (1978).
[41] K. Tatsuka and N. Morimoto, Am. Mineral. **62**, 1101 (1977).
[42] D. L. Abernathy, M. B. Stone, M. J. Loguillo, M. S. Lucas, O. Delaire, X. Tang, J. Y. Y. Lin, and B. Fultz, Rev. Sci. Instrum. **83**, 015114 (2012).
[43] J. Taylor, O. Arnold, J. Bilheux, A. Buts, S. Campbell, M. Doucet, N. Draper, R. Fowler, M. Gigg, V. Lynch, et al., Bull. Am. Phys. Soc. **57** (2012), URL `http://www.mantidproject.org`.
[44] M. Kresch, O. Delaire, R. Stevens, J. Y. Y. Lin, and B. Fultz, Phys. Rev. B **75**, 104301 (2007).
[45] G. Squires, *Introduction to the theory of thermal neutron scattering* (Cambridge University Press, 1978).
[46] P. Brüesch, *Phonons: Theory and Experiments I – Lattice Dynamics and Models of Interatomic Forces* (Vol. 34, Springer Series in Solid-State Sciences, New York, 1982).
[47] E. Makovicky and S. K. Møller, N. Jb. Miner. Abh. **167**, 89 (1994).
[48] A. May, J. Snyder, and J.-P. Fleurial, AIP Conv. Proc., STAIF 2008 **969**, 672 (2008).
[49] A. F. May, J.-P. Fleurial, and G. J. Snyder, Phys. Rev. B **78**, 125205 (2008).
[50] W. Cochran, Adv. Phys. **9**, 387 (1960).
[51] W. Cochran, R. A. Cowley, G. Dolling, and M. M. Elcombe, Proc. R. Soc. London, Ser. A **293**, 433 (1966).
[52] E. Lara-Curzio, A. May, O. Delaire, M. McGuire, X. Lu, C.-Y. Liu, E. Case, and D. Morelli, J. Appl. Phys. **115**, 193515 (2014).
[53] J. W. Andreasen, E. Makovicky, B. Lebech, and S. K. Møller, Phys. Chem. Minerals **35**, 447 (2008).